ACS APPLIED BIO MATERIALS

www.acsabm.org Article

Engineering Bioactive Liposomal Nanoparticles for Kidney-Targeted ECFC Backpacks

Brenda Cruz-Gonzalez, Fei Fan, Eva Hall, Sanjoy Saha, Laura S. Haneline, David P. Basile, and Donny Hanjaya-Putra*

Cite This: https://doi.org/10.1021/acsabm.5c02022 Read Online

ACCESS | Metrics & More | Article Recommendations | Supporting Information

ABSTRACT: Endothelial colony-forming cells (ECFCs) possess significant potential for vascular repair and kidney regeneration but face challenges in selective homing and retention within target tissues. Here, we present a strategy to enhance ECFC targeting to human renal proximal tubular epithelial cells by cell surface engineering with kidney-targeted liposomal nanoparticles conjugated via thiol−maleimide chemistry. These nanoparticles incorporate a targeting peptide that facilitates receptor-mediated binding to renal epithelial cells without altering ECFC phenotypes and cell viability. We demonstrate optimized nanoparticle conjugation and loading that maximizes cellular binding while preserving key progenitor phenotypes and cellular function. Furthermore, the modular nanoparticle design features tunable physicochemical properties conducive to renal targeting and minimal off-target interactions in comparison to fibroblasts. This approach establishes in vitro kidney cell selectivity of surface-engineered ECFCs, laying a foundation for precision nanotechnology to enhance biocompatibility and future organ-specific regenerative therapies.

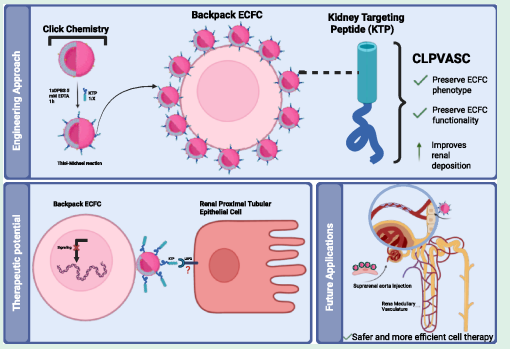

KEYWORDS: *backpack molecules, regenerative medicine, active targeting, nanoparticles, renal delivery, click-chemistry, KTP, endothelial colony-forming cells*

1. INTRODUCTION

Human endothelial colony-forming cells (ECFCs) possess unique advantages due to their critical role in blood vessel development and vascular homeostasis, making them especially valuable for treating cardiovascular and vascular-associated disorders.[1,2] In preclinical studies, ECFCs have demonstrated the ability to enhance vascularization following ischemic stroke, traumatic brain injury, and middle cerebral artery occlusion in the brain, leading to improved blood-brain barrier integrity, reduced apoptosis, and enhanced neurological function.[3−6] In the context of cardiac injury, ECFCs have shown significant benefits after myocardial infarction, including increased neovascularization, improved cardiac function, reduced fibrosis, and decreased apoptosis.[7−10] Additionally, ECFCs have been applied to various vessel-associated conditions such as peripheral artery disease, ischemic retinopathy, and critical limb ischemia, where they have improved vascular function.[7] Their therapeutic potential also extends to acute kidney injury, where factors secreted by ECFCs have been shown to ameliorate ischemia-reperfusion injury, enhance renal medullary blood flow, and decrease immune cell recruitment in animal models.[2] In mice, ECFC treatment resulted in lower plasma creatinine and blood urea nitrogen levels, reduced apoptosis, and less tubular damage.[2,11] Nevertheless, one of the major challenges in ECFC-based therapies is poor engraftment at injury sites.[2,12] In murine hindlimb ischemia models, ECFC retention drops to <5% at 3 days post-injection, with <1% incorporation into perfused vessels by day 7.[13] In renal ischemia-reperfusion injury models, ECFC engraftment is similarly limited (∼2−4% retention at 48 h) due to rapid clearance by macrophages and poor homing.[11,13]

ECFCs mediate renal repair primarily through paracrine effects (VEGF, SDF-1α secretion promoting resident cell survival/angiogenesis) rather than direct vasculogenesis, where sustained local presence is critical.[11,14,15] Even transient retention amplifies therapeutic paracrine signaling 3−5 fold in co-culture models.[16] To leverage ECFC paracrine mechanisms, potent even with transient adhesion, we developed KTP-backpacks, demonstrating enhanced binding selectivity to renal proximal tubule epithelial cells (HRPTEpCs) while preserving ECFC phenotype and functionality. We have achieved this by the membrane modification of the ECFCs, which utilizes the naturally occurring thiol groups on the cell surface, which enable covalent attachment to maleimide-functionalized liposome nanoparticles.

Received: October 11, 2025
Revised: February 18, 2026
Accepted: March 2, 2026

https://doi.org/10.1021/acsabm.5c02022
ACS Appl. Bio Mater. XXXX, XXX, XXX-XXX

These nanoparticles are further modified to display a kidney targeting peptide (KTP), enabling the ECFCs to preferentially home to renal tissue. The thiol-maleimide chemistry ensures a stable, covalent attachment of the nanoparticles, referred to as the "Backpack molecule" approach,[17,18] without compromising the viability or function of the ECFCs.[19] The KTP itself is a short peptide sequence, identified through phage display for its high affinity and specificity to renal vasculature and tubular epithelial cells.[20,21] When conjugated to drug carriers, KTP significantly increases renal deposition, enhances cellular uptake in the kidney, especially in proximal tubule cells,[22] and reduces off-target accumulation in other organs. Recent studies have explored general surface engineering of ECFCs to improve therapeutic potential[23−26]; nevertheless, tissue-specific targeting, especially within the kidney, has been especially underexplored, since the proximal tubule, which is referred to as the "therapeutic window", presents unique homing challenges due to its anatomical barriers and filtration dynamics.[27] The KTP peptide has gotten significant attention as a promising targeting ligand for the kidney's proximal tubule. Here, we developed KTP-targeted ECFCs to evaluate whether this peptide can enhance their therapeutic potential. In this paper, we demonstrate that ECFCs can be effectively modified with targeted liposome nanoparticles using a surface-based targeting technology, which is adaptable for a wide range of regenerative medicine and drug delivery applications.

2. MATERIALS AND METHODS

2.1. Materials

Liposome nanoparticles are composed of lipids: MPB-PE (1,2-dioleoyl-sn-glycero-3-phosphoethanolamine-N-[4-(p-maleimidophenyl)butyramide] (sodium salt)), DOPC (1,2-dioleoyl-sn-glycero-3-phosphocholine), and DOPG (1,2-dioleoyl-sn-glycero-3-phospho-(1'-rac-glycerol) (sodium salt)) were purchased from Avanti Lipids (Alabaster, AL). DiI was purchased from Sigma-Aldrich (St. Louis, MO). KTP peptide (CLPVASCGGK, with a cyclic disulfide bond formed by the two cysteine residues and acetylation at the N-terminus) was synthesized by GenScript (Piscataway, NJ). Pierce Traut's Reagent (2-iminothiolane) and DTNB (Ellman's Reagent, 5,5-dithio-bis-(2-nitrobenzoic acid)) were purchased from ThermoFisher Scientific (Waltham, MA). EDTA (0.5 M), pH 8.0, RNase-free, was obtained from ThermoFisher Scientific (Waltham, MA). UranyLess (22409) was purchased from Electron Microscopy Sciences (Hatfield, PA). Tween-20 was purchased from VWR (Radnor, PA). BSA 30% solution was purchased from VWR (Radnor, PA). Oregon Green 488 Maleimide, Pierce Dilution-Free Rapid Gold BCA Protein Assay, CellMask Plasma Membrane Green, and Hoechst 33342 were all purchased from ThermoFisher Scientific (Waltham, MA). TEM Grids 01813 Carbon Type-B, 300 mesh, Copper were purchased from Ted Pella Inc. (Redding, CA).

2.2. Instruments

Transmission Electron Microscopy (TEM, Talos F200i; ThermoFisher Scientific) was used to confirm nanoparticle nanostructures. ζ-Potential and size distribution values were characterized using a Zetasizer (Malvern Zetasizer Nano ZS; Malvern Instrument Ltd., Worcestershire, U.K.). Nanoparticle Tracking Analysis (NTA; NanoSight LM10 system; Malvern Instrument Ltd., Worcestershire, U.K.) was employed to corroborate nanoparticle size distribution and measure concentration. Confocal Laser Scanning Microscopy (CLSM; Nikon AXR) was used to observe backpack molecule conformation and interactions with cell lines. Fluorescence intensity was quantified using a plate reader (Spark; Tecan, Männedorf, Switzerland). A freeze dryer (Labconco FreeZone 4.5L, Freeze Dryer XL) lyophilized nanoparticle components for subsequent NMR and FTIR analysis. Binding between liposomes and the KTP peptide was analyzed via Fourier Transform Infrared Spectroscopy (Shimadzu IRXross FTIR). A flow cytometer (Cytek NL-2000) assessed peptide-receptor binding and targeted liposome interaction efficiency toward ECFCs. Cell lines were maintained in a HeraCell Vios 160i CO_2 incubator (ThermoFisher Scientific). Sorvall MX120+ Micro-Ultracentrifuge (ThermoScientific) equipped with a Rotor S55-A2 was used to purify liposome nanoparticles.

2.3. Liposome Nanoparticle Synthesis

The synthesis of multilamellar liposome nanoparticles (LNPs) was performed using the standard thin-film lipid hydration method,[28,29] building upon protocols previously established in our laboratory.[24] The components consisted of phospholipids from Avanti Polar Lipids, including MPB-PE(1,2-dioleoyl-sn-glycero-3-phosphoethanolamine-N-[4-(p-maleimidophenyl)butyramide] (sodium salt)), DOPC (1,2-dioleoyl-sn-glycero-3-phosphocholine), DOPG (1,2-dioleoyl-sn-glycero-3-phospho-(1'-rac-glycerol) (sodium salt)), and the fluorescent tracker DiI (1,1′-Dioctadecyl-3,3,3′,3′-tetramethylindocarbocyanine perchlorate, Sigma-Aldrich). To fabricate the LNPs, DOPC, DOPG, MBP-PE, and DiI (1188/303/1890/120 μg) were combined in a glass vial and dried with argon for 5−10 min to obtain a dry lipid film. This film was then hydrated with 1 mL 1× DPBS solution, and the resulting mixture was vortexed ffor 5−7 min.

To improve monodispersity and obtain small liposomal vesicles (<200 nm), the solution was extruded 21 times through a 200 nm polycarbonate membrane using a Mini-Extruder (Avanti Polar Lipids). The extruded solution was incubated at room temperature for 1.5 h to facilitate nanoparticle stabilization, followed by an overnight incubation at 4 °C to ensure complete assembly and maturation of the LNPs to remove unincorporated phospholipids and further purify the LNPs, the solution was subjected to ultracentrifugation at 40,000 rpm and 4 °C for 15 min; this purification step was repeated at least three times to ensure thorough removal of free phospholipids. The final purified LNPs were obtained by resuspending the resulting pellet in 1× DPBS, yielding a stable and homogeneous nanoparticle suspension suitable for downstream applications.

2.4. Liposome KTP Functionalization

To functionalize the LNPs with Kidney Targeting Peptide (KTP, CLPVASCGGK [GenScript]), a thiol-Michael addition reaction was employed. The process involved two main steps: modification of KTP with Traut's reagent and subsequent conjugation to the LNPs. KTP was initially modified with Traut's reagent (2-iminothiolane [ThermoFisher]) at a molar ratio of 1:10, following the ThermoFisher protocol. The reaction took place in a buffer containing 1× DPBS and 5 mM EDTA for 1 h at room temperature. This step converted the primary amine of KTP into a thiol group (KTP-SH), allowing for its attachment to the LNPs. The concentration of thiol groups on KTP-SH was measured using Ellman's assay, which typically yielded approximately 1952 μM of thiol groups. LNPs were characterized using Nanoparticle Tracking Analysis (NTA, [refer to the Section 2.2]) to determine their concentration, typically in the range of 1 × 1011 particles/mL. This analysis also allowed for the estimation of the molar concentration of MPB-PE lipid in the LNPs, usually estimated as 23 μM (Supplementary material). The thiol-Michael addition reaction was carried out by incubating the modified peptide (KTP-SH) with the maleimide-functionalized MPB-PE lipid for 2 h at room temperature, allowing efficient covalent conjugation between the thiol and maleimide groups. Following the reaction, the mixture was subjected to ultracentrifugation at 50,100 rpm and 4 °C for 15 min to separate the conjugated lipid nanoparticles (LNPs) from unreacted free peptide. This purification step was repeated at least three times to ensure thorough removal of excess peptide. The final LNPs were obtained by resuspending the resulting pellet in 1× DPBS. To optimize conjugation efficiency and binding activity, a range of maleimide-to-thiol molar ratios (1:10, 1:30, 1:70, and 1:100) was systematically tested. For residual maleimide quenching to be used

https://doi.org/10.1021/acsabm.5c02022
ACS Appl. Bio Mater. XXXX, XXX, XXX-XXX

in specific binding studies, unreacted maleimide groups on LNPs were blocked with thiol-terminated 2 kDa PEG (mPEG-SH, 1 mg/mL), [Laysan Bio Inc.], for 30 min at room temperature in EGM-2 serum-free medium before specific binding studies.

2.5. Cell Culture

Human Endothelial Colony-Forming Cells (ECFCs) were isolated and characterized using established protocols by IUSM.[28,29] Briefly, Human Mononuclear Cells (MNCs) on collagen I-coated tissue culture plates with complete Endothelial Growth Medium-2 (EGM-2). After 24 h, non-adherent cells were removed, and fresh EGM-2 was added. Endothelial cell colonies, appearing as cobblestone-like monolayers, emerged between days 5 and 8. ECFCs were characterized by flow cytometry based on their surface antigen profile. Cells were defined as ECFCs by positive expression of CD31, CD141, CD105, CD144, von Willebrand factor (vWF), and Flk-1, and by the absence of hematopoietic markers CD41 and CD14. The proliferative potential was assessed through single-cell colony-forming assays. Indiana CTSI did the isolation protocol. For ongoing culture, surfaces were pre-coated with a rat-tail collagen type I (RTC1) solution, incubated, and then washed with 1× DPBS. The growth medium consisted of EGM-2 supplemented with Mix (PromoCell) and mycoZap Prophylactic (Lonza).

Human Renal Proximal Tubular Epithelial Cells (HRPTEpCs) were purchased from Cell Applications and cultured in RenaEpi medium supplemented with mycoZap Prophylactic (Lonza). Human Pulmonary Fibroblasts (HPFs), Blood Endothelial Cells (BECs), and Human Umbilical Vein Endothelial Cells (HUVECs) were obtained from PromoCell and cultured on tissue culture plates. HPFs were maintained in FGM2 medium; HUVECs in EGM-2 supplemented with Mix (PromoCell) and cultured in collagen I-coated tissue culture plates; and BECs in EGMV-2 supplemented with Mix (PromoCell). All cell lines were cultured at 37 °C with 5% CO_2, passaged using DetachKit (PromoCell), and used for experiments between passages 5−8. Regular mycoplasma testing confirmed all cultures remained negative throughout the study. Further details on the cell lines are provided in Table S1 of the Supplementary Material.

2.6. Conjugation of Peptide-Liposome Nanoparticles to ECFCS

KTP-functionalized liposome nanoparticles (LNPs@KTP) and LNPs were conjugated to the surface of ECFCs by incubating equal volumes of ECFCs and LNPs@KTP in complete EGM-2 medium at a ratio of 1:5000 (cell: nanoparticles). The mixture was incubated for 30 min at 37 °C under gentle agitation to facilitate covalent conjugation between maleimide groups on the liposomes and free thiols on the ECFC surface. Successful conjugation was verified via confocal microscopy using DiI-labeled LNPs (red fluorescence) and CellMask Plasma Membrane Green (cell membrane staining). Quantitative assessment of surface-bound nanoparticles was performed by flow cytometry (Cytek NL-2000), with mean fluorescence intensity (MFI) analyzed using FlowJo software (v10.8.1).

2.7. In-Vitro Nanoparticle-Cell Interaction Assays

ECFCs, HRPTEpCs, and HPF at passages 7–10 were evaluated for in vitro nanoparticle-cell interactions using quantitative flow cytometry[19] and confocal laser scanning microscopy (CLSM),[18] following established protocols. These complementary techniques enabled both the quantitative measurement and spatial visualization of nanoparticle binding and localization on the cell surface.

2.7.1. Flow Cytometry Analysis. Cells were harvested by incubating with the Detach Kit (PromoCell) for 3–5 min at 37 °C. Cell dissociation was neutralized with TNS, followed by centrifugation and washing with FACS buffer (PBS containing 2% FBS). Cell pellets (approximately 1 × 106 cells per sample) were resuspended for subsequent staining procedures. For blocking experiments, cells were incubated with 2% BSA at 4 °C for 2 h, protected from light, and then washed with FACS buffer three times. For the maleimide blocking technique, cells were incubated with 5.5 μM Maleimide C5 Oregon Green (FITC) per 1×10^6 cells for 15 min, as previously described,[15] to block surface thiol groups. After blocking, cells were incubated with fluorophore-conjugated LNPs or LNPs@KTP (at a 1:5000 cell-to-LNP ratio, unless otherwise specified) for 30 min at 37 °C with continuous agitation, protected from light. Appropriate controls were included: PE-conjugated liposome nanoparticles (LNP alone), unstained cells, and FITC-conjugated, non-treated cells for the maleimide blocking control. Following incubation, cells were washed twice with FACS buffer. Data acquisition was performed on a Cytek NL-2000 flow cytometer.

2.7.2. Proliferation Assay. ECFCs (2.5×10^5 cells/well in 6-well plates) were stained with 20 ng/mL CFSE (Thermo Fisher) for 15 min at 37 °C, washed, and cultured for 1, 2, and 3 days. Proliferation was assessed by flow cytometry (Cytek NL-2000), quantifying CFSE dilution in live singlets.

2.7.3. Phenotypic Analysis (CD31 Expression). ECFCs (2.5 × 105 cells/well in 6-well plates) were harvested, blocked with 2% BSA (2 h, 4 °C), and stained with Human CD31-APC (1:100, Bio-Techne) or mouse IgG1-APC isotype control (1:100, Bio-Techne) for 30 min at 4 °C. Cells were washed and analyzed by flow cytometry as above to confirm preserved endothelial phenotype (>95% CD31+ post-backpacking).

A standard gating strategy was used: first, cells were gated by forward (FSC-A) and side scatter (SSC-A) to exclude debris; singlets were then selected using FSC-A versus FSC-H to exclude doublets (Supplementary Figure S1). The live, singlet population was analyzed for LNP-positive binding. Data analysis was performed using FlowJo software (SpectroFlo, Version 3.3.0).

2.7.4. Binding Backpacks to ECFCs. Backpacks were quantified using a hemocytometer, and 3.75 × 104 backpacks were added per well to a 96-well ultra-low attachment plate (rounded bottom). Cells were stained with Cell Plasma Green (1:1000) and Hoechst (1:2000) for 10 min at room temperature, followed by three washes with basal media. After a 15-min rest period, LNPs or LNPs@KTP were added at a 1:5000 cell-to-backpack ratio and incubated for 30 min at 37 °C with continuous shaking. Cells were washed three times with basal media, fixed with 4% PFA, and transferred to a 24-well plate. The plate was centrifuged at 300 × *g* for 7.5 min to sediment backpacks for confocal microscopy analysis, similar to previous published literature.[18]

2.7.5. Uptake Study. HUVECs and BECs were seeded in T75 flasks and cultured until reaching full confluency. Once confluent, cells were passaged onto 24-well plates coated with RTC1. After allowing cells to attach, various LNP formulations were added at a cell-to-nanoparticle ratio of 1:5000. The plates were placed on a shaker inside a 37 °C incubator for 5 h. Following the incubation, nanoparticles were removed by washing the cells three times with 1× DPBS, and the cells were then fixed for 15 min using 3.7% paraformaldehyde. Imaging was performed the next day using confocal microscopy, with fresh 1× DPBS maintained in the wells during imaging.

2.7.6. Live/Dead Viability Assay. ECFCs (0.04×10^6 cells/well in black-bottom 96-well plates) were treated with LNPs@KTP at varying KTP ratios (1:10 to 1:100) for 24 h in complete growth medium. Following treatment, medium was removed, and cells were stained using the LIVE/DEAD Viability/Cytotoxicity Kit (Thermo Fisher) per manufacturer's protocol. Briefly, 5 μL calcein AM (Component A) and 20 μL ethidium homodimer-1 (Component B) were added to 10 mL DPBS to prepare the staining solution. Cells were incubated with 100–200 μL staining solution for 30 min at 20–25 °C, protected from light. Live (green fluorescence, intact membranes) and dead (red fluorescence, compromised membranes) cells were imaged using fluorescence microscopy (Nikon AXR confocal). Viability was quantified as % live cells (>95%

https://doi.org/10.1021/acsabm.5c02022
ACS Appl. Bio Mater. XXXX, XXX, XXX-XXX

across all ratios, Supplementary Figure S6; $n = 3$ wells/condition), code available in the Supplementary Material.

2.7.7. Vascular Tube Formation Assay. Vascular tube formation was performed as previously reported.[23,35,36] Briefly, 15-well μ-angiogenesis plates (ibidi) were placed at −80 °C for ≥2 h to cool. On ice, 10 μL Matrigel was added per well, and plates were placed in a petri dish with 1−2 mL PBS, then incubated at 37 °C, 5% CO_2 for 2 h to polymerize. ECFCs (backpacked or untreated; 50 μL cell suspension at 80,000 cells/mL) were added per well. Plates were imaged at 4× and 10× magnification for 1−5 h using the ECHO Revolve Fluorescent Microscope. Images were pre-processed and quantified using the AutoTube.[36,37]

2.8. Statistics and Reproducibility

Data are presented as mean ± standard deviation unless otherwise specified in the figure legends. Sample sizes were determined by power analysis using a 95% confidence interval to ensure adequate statistical power for detecting significant differences. The number of samples used in each experiment was sufficient to achieve a normal distribution. All statistical analyses were performed using GraphPad Prism software. For flow cytometry (FACS) data, statistical comparisons were conducted using one-way ANOVA followed by Dunnett's post-hoc test. For quantification of KTP in BCA assays and relative fluorescence units (RFU), unpaired t-tests were employed. Statistical analysis of live/dead assay data from five LNP treatment groups (A−E, total $n = 40$) showed significant viability differences by one-way ANOVA ($F(4,35) = 9.851$, $P < 0.0001$, $R^2 = 0.5296$), with treatments explaining ∼53% of variance. Variance homogeneity was confirmed by Brown-Forsythe ($P = 0.4655$) and Bartlett's ($P = 0.3915$) tests, validating the normal distribution assumption for ANOVA. To quantify the nanoparticles per cell difference across ratios of the backpack molecules, one-way ANOVA analysis of your 5 treatment groups (A−E) showed no statistically significant differences in nanoparticle uptake (Red/DAPI ratios). The treatments explained only 19% of data variation ($R^2 = 0.19$), while random biological variation dominated. Variance tests (Brown-Forsythe $P = 0.56$) confirmed equal spreads across groups, indicating that the conditions performed similarly with current data variation. Statistical significance was defined as follows: $*P < 0.05$, $**P < 0.01$, $***P < 0.001$, and $****P < 0.0001$.

3. RESULTS

3.1. Rational Design and Synthesis of Kidney-Targeting Nanoparticles

We engineered the CLPVASCGGKpep-targeted liposome nanoparticles (LNPs@KTP) by modifying the cyclic-KTP peptide with Traut's reagent to enable maleimide-thiol click chemistry conjugation (Figure 1A,B; Section 2). The final nanoparticle formulation consists of four functional components: (1) MPB-PE, which serves as both the anchor for KTP peptide conjugation via its maleimide head group and as a linker to thiol groups on ECFC membranes, while also contributing to membrane permeability and tunable peptide attachment[30−32]; (2) DiI fluorescent lipid dye for imaging and tracking, chosen for its strong membrane incorporation and reliable fluorescence properties[33]; (3) DOPC, which provides membrane flexibility due to its unsaturated acyl chains, supporting fluid phase behavior[34]; and (4) DOPG, which imparts colloidal stability and a negative surface charge, enhancing interaction with positively charged molecules and improving encapsulation stability.[35] Nanoparticles were synthesized from pure components using precise stoichiometric ratios to ensure consistent targeting peptide density across batches, resulting in homogeneous populations with controlled placement of targeting elements at defined molar ratios (Figure 1C). Following extrusion through 0.2 μm membranes to form multilamellar liposomes, the nanoparticles displayed a uniform hydrodynamic size distribution as verified by dynamic light scattering (Figure 1D,E). This rational design enables active and specific renal targeting through the KTP motif, ensuring reproducible experimental outcomes by maintaining precise control over nanoparticle composition and surface functionalization.

3.2. Comprehensive Characterization of KTP-LNPs

To further validate our nanoparticle design, we conducted a comprehensive, multi-modal characterization of KTP-LNPs (Figure 2, Supplementary Figure S2). Transmission electron microscopy (TEM) confirmed that the nanoparticles displayed uniform, spherical morphology and consistent size, which are critical for predictable in vivo performance and biodistribution (Figure 2A).[36] Nanoparticle tracking analysis (NTA) provided a quantitative assessment of particle concentration and size distribution, ensuring reproducibility and enabling accurate dosing (Figure 2B).[37]

For peptide quantification, we employed both the bicinchoninic acid (BCA) assay (Figure 2C) and fluorometry using FITC-labeled KTP (Figure 2D). While the BCA assay is traditionally used for proteins, it can also quantify peptides containing sufficient peptide bonds and side chains capable of reducing Cu^{2+}, making it suitable for our application.[38] For this technique, three washes with 1× DPBS were performed to purify KTP from the LNPs. Each purification step was monitored using the BCA protein assay to ensure complete removal of unbound peptide. This process involves micro ultracentrifugation, allowing for efficient separation and confirmation of successful purification (Supplementary Figure S3). In parallel, fluorometric measurements were performed using a plate reader, with a calibration curve constructed from known concentrations of FITC-KTP (Supplementary Figure S4). This enabled back-calculation of the KTP content in micromolar units, which showed good agreement with the BCA results, providing validation of peptide loading.

Zeta potential analysis revealed that our liposome formulations possessed a moderately negative surface charge, primarily due to the presence of DOPG and the phosphate head groups of DOPC and MPB-PE (Figure 2E). Upon addition of the KTP peptide, the negativity increased, likely reflecting the net negative charge of the peptide at physiological pH. This increased negativity enhances colloidal stability by promoting electrostatic repulsion between particles and may also reduce nonspecific uptake by non-targeted cells, thereby improving targeting specificity.[39]

Fourier-Transform Infrared spectroscopy (FTIR) was employed to confirm successful KTP conjugation (Figure 2F−H). The spectra showed characteristic peaks corresponding to the amide C=O stretch, and the nitrile (−CN) group,[40] all indicative of the peptide's presence and its covalent attachment to the liposome surface. The detection of the amide C=O and −CN stretches is consistent with peptide backbone and side-chain functionalities (Figure 2G), further validating the integrity of the conjugation chemistry. The single, broader peak in the FTIR amide I region after conjugation may indicate a less well-defined or more heterogeneous secondary structure population for KTP on the nanoparticle surface.[41] This is common when peptides are immobilized or interact with lipid surfaces, as the local environment disrupts or averages their secondary structure, making specific α-helix or β-sheet features less distinct in the spectrum.

https://doi.org/10.1021/acsabm.5c02022
ACS Appl. Bio Mater. XXXX, XXX, XXX-XXX

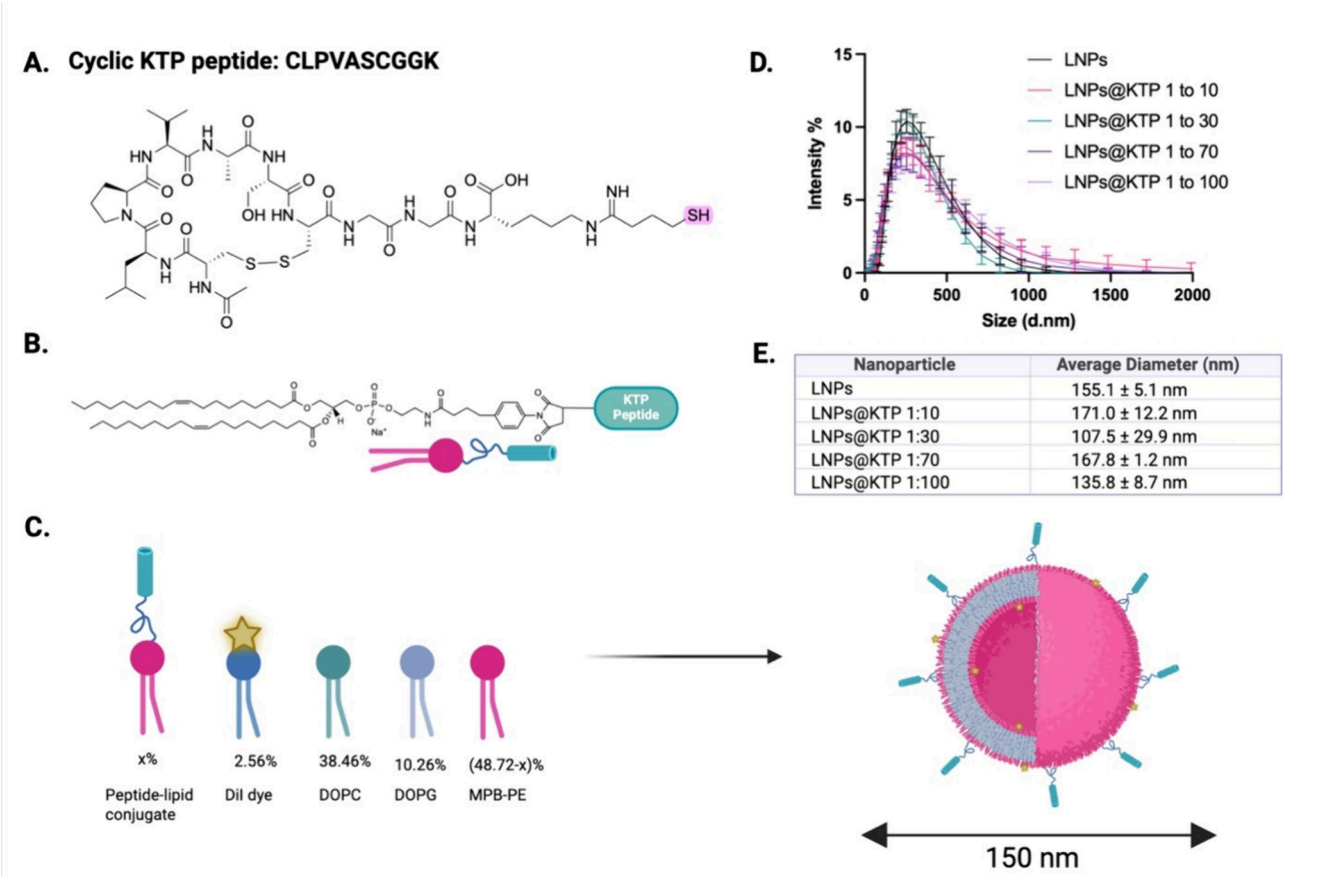

Figure 1. Synthesis and characterization of kidney-targeting peptide (KTP)-conjugated liposomal nanoparticles (LNPs) via click chemistry: (A,B) Schematic of maleimide-thiol conjugation strategy. (C) Liposome composition by the molar ratio. (D,E) Hydrodynamic size distribution by dynamic light scattering.

These results demonstrate robust and reproducible synthesis of LNPs@KTP, with precise control over peptide loading and surface chemistry, key parameters for effective targeting and delivery. The combination of BCA and fluorometric assays provides confidence in peptide quantification, while the observed increase in negative surface charge and the FTIR signatures confirm successful functionalization. This thorough physicochemical characterization is essential for ensuring batch-to-batch consistency, scalability, and translational potential of kidney-targeted nanomedicines.

3.3. Optimization of ECFC–Nanoparticle Interactions

We utilize a thiol-Michael addition (i.e., click chemistry) reaction to couple LNPs to ECFCs. In this system, the maleimide group, introduced via the MPB-PE component of the liposome, reacts specifically with thiol groups that are naturally present on the ECFC membrane (Supplementary Figure S5). This chemistry enables efficient and stable conjugation of LNPs onto the cell surface.

Similarly, for functionalizing LNPs with the KTP peptide, we employ the same maleimide-thiol click reaction. Here, maleimide groups on the LNPs react with thiol groups introduced into the modified KTP peptide (KTP-SH), allowing successful and site-specific attachment of the peptide to the nanoparticle surface.

Because both the ECFC attachment ("backpack" formation) and KTP peptide conjugation rely on the same type of reactive group (maleimide) on the LNP, careful balance is required. To avoid compromising the ability of the LNPs to bind ECFCs after KTP modification, it is essential to determine the maximum loading of KTP that maintains an adequate number of available maleimide groups for subsequent ECFC binding. Over-saturating the LNP surface with KTP could reduce or block the remaining maleimide groups, hindering backpack formation and efficient cell-nanoparticle conjugation.

To address this question, we conducted flow cytometry analysis to evaluate the binding efficiency of various LNP@KTP formulations with ECFCs (Figure 3A). By systematically comparing different KTP-to-LNP ratios, we identified that optimal binding occurs in the range of 1:10 to 1:70 LNPs@KTPs. Notably, when the ratio was increased to 1:100, we observed a marked decrease in binding efficiency (Figure 3B). This reduction suggests that, at higher ratios, the maleimide (MAE) groups on the LNP surface become saturated with KTP peptide, which in turn impairs the ability of the LNPs to interact effectively with ECFCs. These findings highlight the importance of optimizing the KTP-to-LNP ratio to balance peptide modification with cell-binding functionality for our application.

These results were further substantiated using confocal microscopy, which confirmed the successful formation of the "backpack" structures. In this analysis, cell nuclei were stained with Hoechst, and the cell membrane was labeled using a green cell tracker dye. The "Backpacks", corresponding to the LNPs@KTP, were visualized in red due to DiI fluorescence from the liposome nanoparticles. As shown in Figure 3C–E, these images demonstrate that LNPs conjugated with the targeting agent KTP are localized specifically on the membrane of ECFCs, validating effective surface conjugation and "backpack" assembly, validating a robust

https://doi.org/10.1021/acsabm.5c02022
ACS Appl. Bio Mater. XXXX, XXX, XXX-XXX

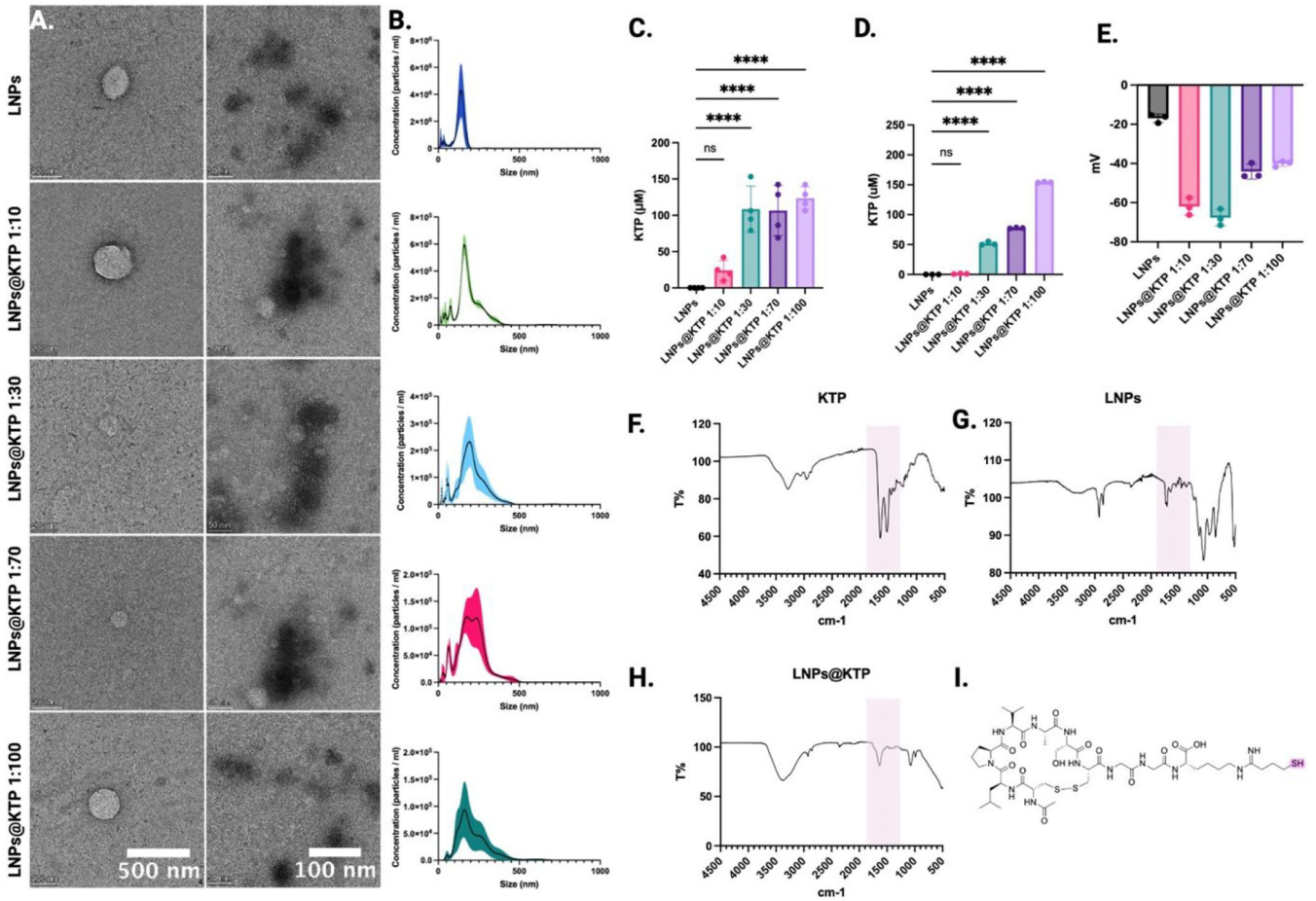

Figure 2. A comprehensive characterization of kidney-targeting peptide (KTP) loading on liposome nanoparticles (LNPs) was performed using multiple analytical techniques. (A) Transmission electron microscopy (TEM) was used to assess nanoparticle size and morphology, while (B) nanoparticle tracking analysis (NTA) quantified particle concentration in particles per milliliter. (C) The amount of the encapsulated peptide was determined by a BCA assay, and (D) the molarity of surface-conjugated KTP was quantified using fluorometry with the FITC-labeled peptide. (E) Zeta potential analysis was conducted to evaluate the interaction potential of the LNPs with cellular and biological membranes. (F−H) FTIR spectroscopy was used to verify the successful conjugation of KTP to the liposomes by identifying characteristic spectral peaks. (I) CLPVASCGGK (M_W 974.16 Da; N-terminal acetylation, disulfide bond between Cys1-Cys8). The terminal lysine "K" enables Traut's reagent modification to generate a free thiol for site-specific maleimide conjugation to LNPs, while the native cysteines form the stable disulfide loop.

cell-nanoparticle interaction. This study underscores the importance of modulating KTP loading to ensure dual functionality, a targeted system, and effective cell attachment.

To further analyze the impact on viability when altering the ECFCs with a slightly modified moiety, we performed a live/dead assay. The core mechanism of the live/dead assay is to exclude live cells from the impermeant "dead" dye while taking up the live dye, where dead cells fluoresce red only. In our nanoparticle contexts, our LNP@KTP on ECFCs showed a >90−95% green/live staining, which confirms no cytotoxicity across ratios, Supplementary Figure S6.

To assess the impact of backpacking on ECFC proliferation, cells were treated with LNPs@KTP at the optimized ratios (1:30 and 1:70), stained with CFSE, and monitored over 3 days. ECFCs showed no significant differences in CFSE dilution profiles compared to untreated controls, confirming preserved proliferative capacity post-backpacking. Figure 4A.

To investigate the impact on the phenotypic alteration of the backpack ECFCs, CD31 (PECAM-1), a canonical endothelial marker constitutively expressed on ECFCs,[42] was assessed to confirm backpacking does not alter endothelial identity, as no ECFC-specific markers exist and phenotypic stability is critical for therapeutic translation.[1] Post-backpacking ECFCs showed no significant change in CD31-APC expression compared to non-treated controls (>95% CD31+ both conditions; $n = 2$). Figure 4B.

To evaluate functional preservation post-backpacking, ECFCs (backpacked or untreated) were seeded on μ-angiogenesis plates and monitored for 5 h. Tube formation initiated indistinguishably between treated and non-treated cells at 2−4 h, with no significant differences in tube width, tube area, branch number, hull area, or skeleton length ($n = 3$), Figure 4 D−I.

These results collectively demonstrate that KTP-LNP backpacking preserves ECFC proliferation, endothelial phenotype, and angiogenic functionality comparable to untreated controls (Figure 4). Surface modification thus maintains therapeutic potency while enabling kidney cell selectivity.

3.4. Selective Targeting of Renal Epithelial Cells by KTP

To assess HRPTEpC selectivity and rule out non-specific interactions, LNPs were PEGylated by quenching residual maleimide groups with thiol-terminated 2 kDa PEG (as

https://doi.org/10.1021/acsabm.5c02022
ACS Appl. Bio Mater. XXXX, XXX, XXX-XXX

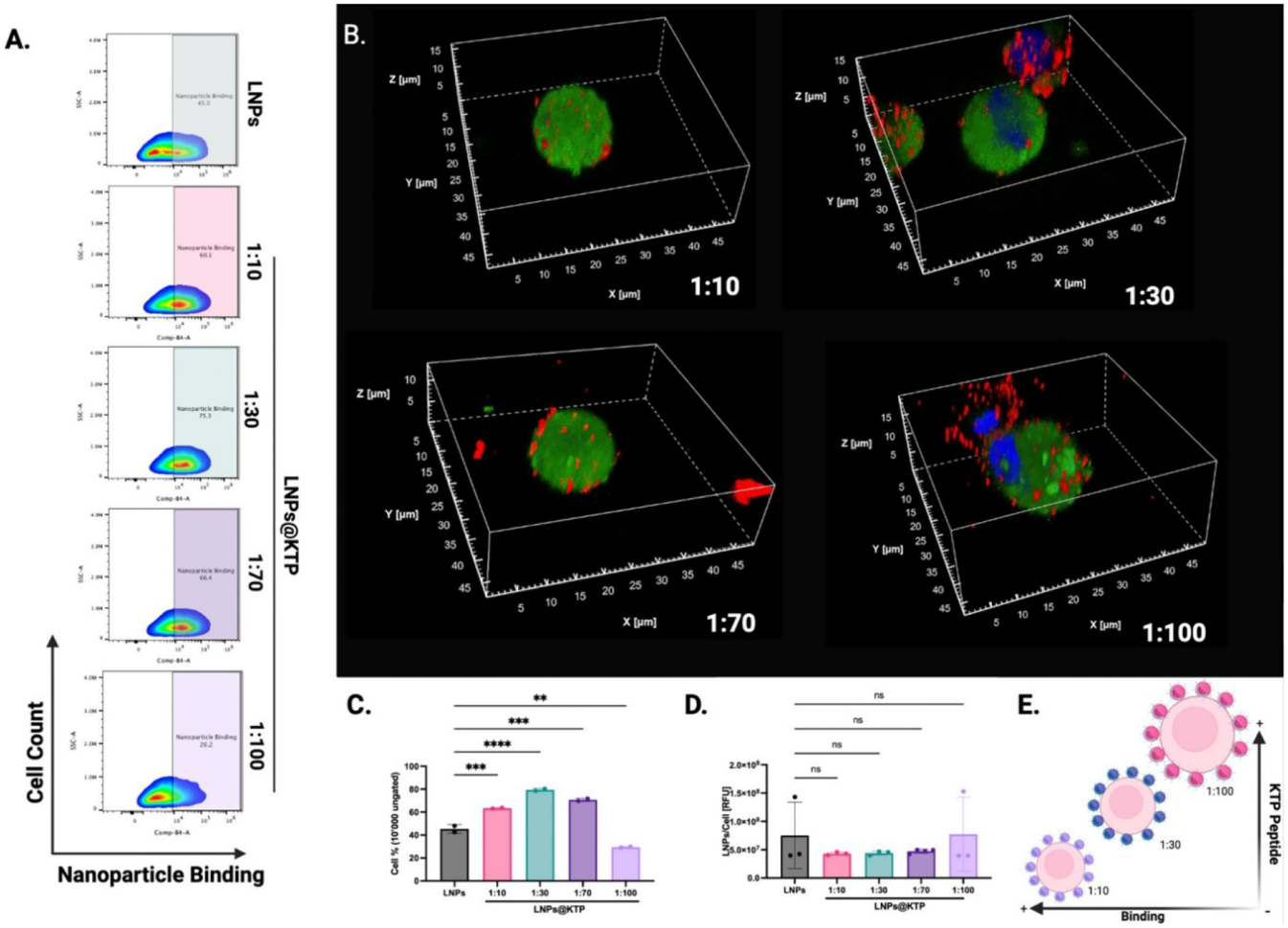

Figure 3. Characterization of ECFC binding as a function of the KTP-to-LNP ratio. (A) Flow cytometry was used to determine the saturation point of ECFC surface binding by LNPs functionalized with increasing KTP-to-LNP ratios. (B) Representative 3D confocal reconstructions illustrate membrane-associated LNPs on ECFCs across these formulations. (C) Quantification of the flow cytometry data shows the relationship between the KTP-to-LNP ratio and ECFC surface occupancy. (D) Quantification of the 3D reconstructions demonstrates that all ratios achieve a comparable nanoparticle load, corresponding to an approximate 1:5000 cell-to-nanoparticle ratio. (E) Schematic representation of the interaction between ECFCs and the targeting moiety, illustrating that excessive KTP decoration of the nanoparticles leads to loss of ECFC binding and, consequently, loss of the "backpack" configuration.

described in Section 2). This nanoparticle-side blocking strategy, mirroring the maleimide-thiol competition used for ECFC surface modification, eliminates non-covalent binding, confirming covalent KTP conjugation dominates, while demonstrating PEGylation prevents non-specific nanoparticle-HRPTEpC interactions. Cell-side blocking controls were also employed as follows. Maleimide (MAE) blocking, based on the known reactivity between MAE groups on the LNPs and thiol groups present on cell membranes (Figure 5A,F). This approach helps distinguish specific targeting by the KTP ligand from nonspecific thiol-based interactions. The second strategy used bovine serum albumin (BSA) blocking. BSA is a highly adsorptive molecule that binds broadly to surfaces through non-specific interactions, serving as a general blocking agent to reduce non-selective binding. By applying both blocking strategies, we aimed to determine whether KTP present on the LNPs functions as a true targeting ligand-engaging in receptor-mediated interactions with HRPTEpCs, rather than relying on nonspecific surface adherence.

In these studies, we observed baseline, or "basal", binding of LNPs to HRPTEpCs at approximately 48.8% of the total cell population under MAE blocking conditions, and 63.7% with BSA blocking. When KTP was incorporated into the LNP design, binding significantly increased-reaching 86.6% with MAE blocking and 95.4% with BSA blocking (Figure 5A). These findings demonstrate a clear enhancement in cell binding mediated by the KTP modification, as confirmed by significant differences between the control LNPs and KTP-functionalized LNPs (Figure 5C,D). To validate the specificity of this targeting, we conducted parallel experiments using human pulmonary fibroblasts (HPFs) as a negative control. Blocking was not applied to this cell line, as fibroblasts and epithelial cells display distinct surface phenotypes, and KTP is not expected to target fibroblasts.

As expected, there were no significant differences in binding between control and KTP-modified LNPs-except for the 1:10 formulation, where the observed increase was attributed to non-specific interactions between unreacted maleimide groups on the nanoparticles and thiol groups present on the HPF surface

https://doi.org/10.1021/acsabm.5c02022
ACS Appl. Bio Mater. XXXX, XXX, XXX-XXX

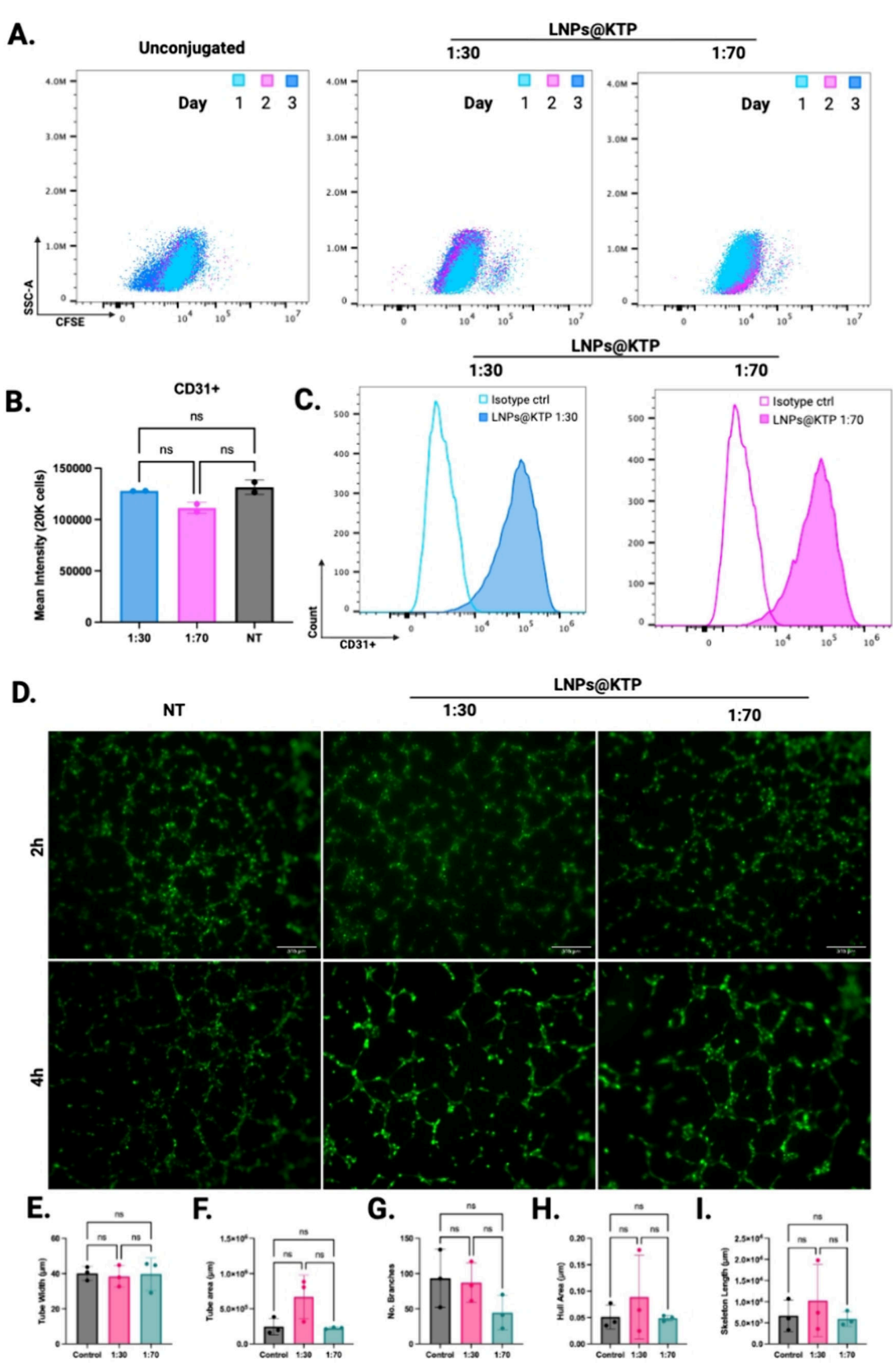

Figure 4. Functional preservation of KTP-LNP backpacked ECFCs. (A) CFSE proliferation assay tracking ECFC division over 3 days for optimized backpack ratios (1:30, 1:70) vs non-treated (NT) controls. (B) CD31-APC expression confirming preserved endothelial phenotype post-backpacking vs NT (>95% CD31+). (C) CD31 expression relative to isotype controls. (D) CFSE-stained tube formation assay (2 h, 4 h) comparing backpacked ECFCs (1:30, 1:70) vs NT. (E–I) Quantification of tube formation metrics (tube width, tube area, branch number, hull area, skeleton length, $n = 3$). Scale bar = 320 μm.

https://doi.org/10.1021/acsabm.5c02022
ACS Appl. Bio Mater. XXXX, XXX, XXX-XXX

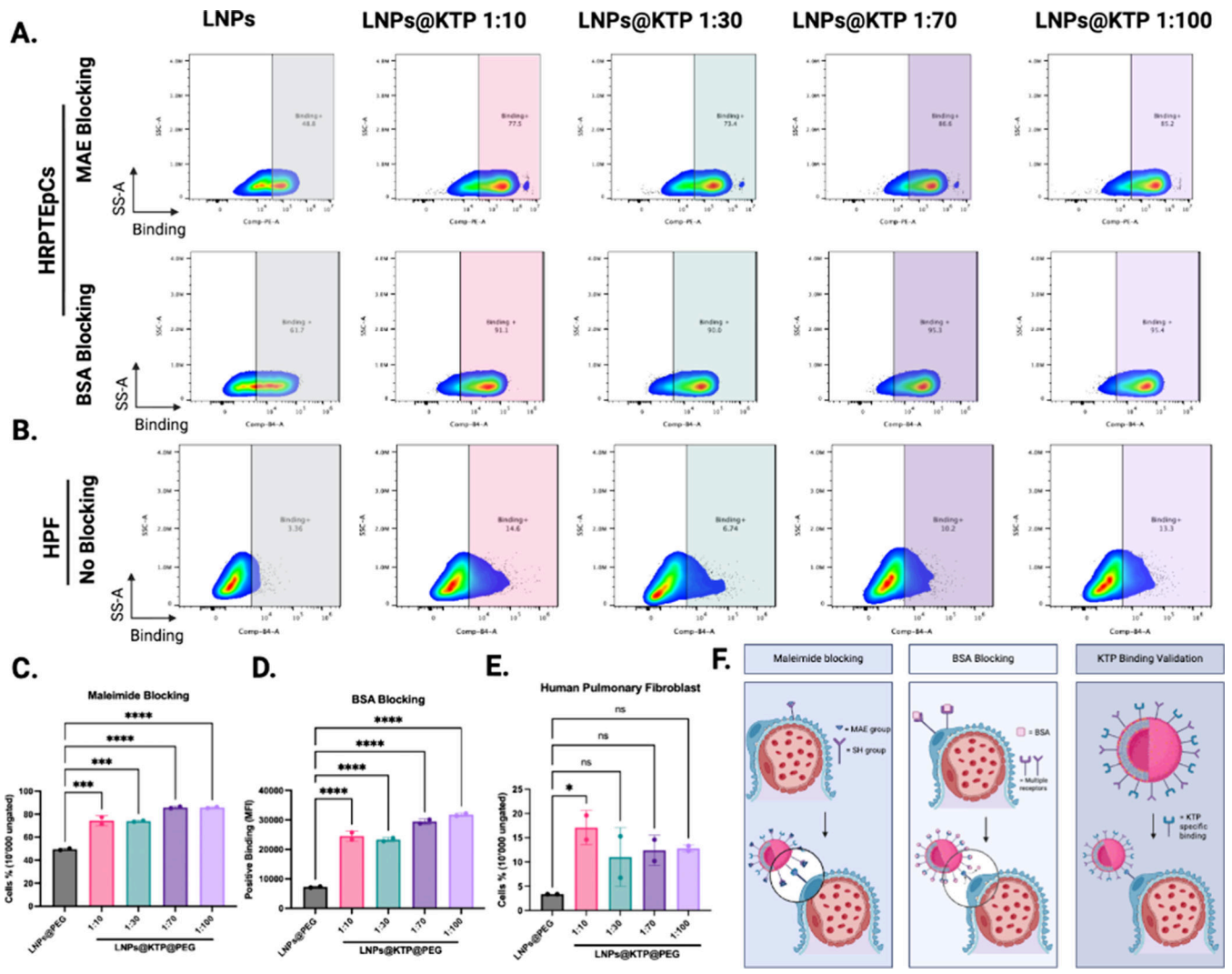

Figure 5. Increased binding of KTP-functionalized nanoparticles to HRPTEpCs when compared to non-targeted LNPs, as measured by flow cytometry. Under both MAE blocking (A,C) and BSA blocking (A,D) conditions, KTP modification leads to a pronounced rightward (red) shift in fluorescence intensity, indicating higher cell association relative to the baseline established by non-targeted LNPs. In contrast, when human pulmonary fibroblasts (HPFs) were used as a control cell line, there was no significant increase in nanoparticle binding with KTP modification, even in the absence of blocking treatments (B,E). These results demonstrate the selective affinity of KTP for renal epithelial cells over non-targeted nanoparticles and confirm that KTP provides targeted binding specificity, distinguishing kidney epithelial cells from unrelated cell types. (F) Schematic of experimental design showing HRPTEpC cells (blue) and ECFCs (red), with blocking strategies using MAE (maleimide competition) and BSA (nonspecific binding control) and their mechanisms.

(Figure 5E, Supplementary Figure S5). The KTP peptide is a well-suited candidate for selective targeting of kidney epithelial cells, with its effectiveness previously demonstrated in other constructs such as ELPs.[17] Crucially, our findings show that the KTP peptide does not solely target epithelial cells, it also enables robust binding to endothelial cells, broadening its potential application for technologies aimed at both kidney tubules and vasculature.

4. DISCUSSION

The kidney-targeting peptide KTP represents a promising, yet underexplored ligand originally discovered through in vivo phage display biopanning by Pasqualini and Ruoslahti, identifying its remarkable 120-fold renal proximal tubule selectivity.[43] Despite demonstrated efficacy across nanoparticles, biopolymers, and liposomes,[20−22,44,45] KTP's biochemical characterization remains limited. While our data confirm functional kidney cell tropism (3.2-fold HRPTEpC selectivity), the "black box" nature of KTP binding underscores a critical knowledge gap. Future biochemical studies, receptor pull-downs, structural modeling, and epitope mapping could unlock rational KTP engineering, enhancing specificity for clinical translation beyond empirical successes like our ECFC backpacking strategy.

In our studies, the 1:30 (KTP:LNP) formulation exhibited a reduced hydrodynamic diameter (107.5 ± 29.9 nm) compared to other ratios (130−200 nm), representing ∼30% size decrease. This compaction likely reflects optimal maleimide-thiol stoichiometry, enabling efficient surface crosslinking without excess peptide crowding.[46,47] Higher ratios (1:70, 1:100) showed expanded diameters, potentially due to unreacted thiol chains extending the solvation layer. The compact 1:30 nanoparticles may offer enhanced steric accessibility for ECFC membrane association,

https://doi.org/10.1021/acsabm.5c02022
ACS Appl. Bio Mater. XXXX, XXX, XXX-XXX

while all formulations achieved equivalent 1:5000 cell: NP loading, supporting their suitability for backpack-mediated kidney targeting.

PEG coating is a common strategy to stabilize nanoparticles and improve biocompatibility. In our work, we used PEG-SH to quench excess maleimide groups on MPB-PE liposomes, confirming that covalent KTP attachment drives kidney cell selectivity. Un-PEGylated LNPs showed non-specific binding to HRPTEpCs (data not shown), while PEGylation eliminated this off-target interaction. This proves specific KTP-mediated targeting and creates backpacks that reach the kidneys without non-specific effects, in addition to our BSA and MAE blocking strategies.

Previous studies in our laboratory demonstrated that liposomal nanoparticles with tunable release kinetics can be conjugated onto ECFCs to enhance their therapeutic potential, particularly by restoring impaired cell migration and vasculogenesis in ECFCs affected by gestational diabetes mellitus. This supports the usefulness of the new technique for therapeutic strategies by effectively delivering agents to improve ECFC function.[48,49] Additionally, this study also exhibits that the liposomes remained stable for at least 30 days when stored at both 4 and 37 °C, making them suitable for long-term storage and clinical applications. Moreover, this cell line has demonstrated minimal inflammatory responses following in vivo implantation, highlighting their biocompatibility and safety for potential clinical applications.[20] Therefore, our study aims to create a biomaterial that potentially could facilitate the clinical translation of the ECFCs by introducing a kidney-targeting peptide into the system, which will be referred to as "Molecular Backpacks".

To create the "backpacks" (nanoparticles conjugated to cells), it has been determined that approximately 5000 ± 100 liposomal particles could be attached to the surface of each ECFC without negatively affecting cell viability or proliferation.[19] Nanoparticle attachment covers only ∼5% of a typical 20 μm cell surface. This low coverage preserves cell function while adding targeting ability.[32] This approach matches Dr. Mitragotri's 'backpack' work. His team attached disc-shaped polymers to macrophages to improve targeting and therapy.[18] Our KTP-LNPs use the same idea but with liposomes on ECFCs. This technology demonstrates how surface-conjugated biomaterials can modulate cell behavior and improve the efficacy of targeted, cell-based treatments.[13]

A key requirement for backpack molecules is proving that nanoparticles remain mainly on the therapeutic cell surface. This is challenging because nanoparticle shape, spherical, rod, star, or disc, predicts the engulfment.[36] However, internalization can compromise cell phenotype, viability, and function. Previous studies show that surface-attached liposome nanoparticles, like those in the present work, can distribute evenly between daughter ECFCs during cell division.

These nanoparticle-conjugated ECFCs maintain key markers, CD31, CD34, and CD144, at levels comparable to unmodified cells.[19] This demonstrates that our nanoparticle design itself does not compromise ECFC phenotype or essential functions. In this subsequent study, we evaluated key ECFC characteristics post-KTP-liposome backpacking: Live/Dead staining confirmed >95% viability; CFSE tracking showed undistinguishable proliferation over 3 days; CD31-APC flow cytometry verified preserved endothelial phenotype (>95% CD31+ vs untreated, $n = 3$, $p > 0.05$), as CD31 is a canonical endothelial marker alongside CD34/CD144 whose stability confirms phenotypic integrity absent ECFC-specific alternatives[50]; and tube formation assays (2−4 h, CFSE-stained) revealed no differences in tube width, area, branches, hull area, or skeleton length ($n = 3, p > 0.05$). These data collectively demonstrate that KTP modification maintains ECFC therapeutic functionality.

When evaluating how KTP interacts with other cell lines, it is important to note that KTP d−emonstrates a variable and cell-type-specific binding profile. Significant differences in cellular uptake are observed with KTP conjugation ratios of 1:10 and 1:30, while higher ratios (1:70 and 1:100) result in diminished statistical significance. We hypothesize that two mechanisms contribute to nanoparticle uptake: active targeting via KTP and passive targeting through maleimide-activated end groups (MAE) interacting with thiol groups on the endothelial cell membrane. At high conjugation ratios, such as 1:100, the majority of maleimide sites are occupied by KTP, limiting the potential for passive interactions and leaving only KTP-mediated targeting. Regarding the absence of significant differences at the 1:70 ratio, it is possible that this intermediate level of KTP conjugation leads to a suboptimal balance between active and passive targeting mechanisms. At this ratio, there may be insufficient KTP density for maximal active targeting, but also reduced passive interaction due to partial occupancy of maleimide sites. This could result in uptake levels similar to the control, eliminating statistical significance. These findings align with our previous results, where excessive KTP conjugation similarly impaired ECFC backpack formation, reinforcing the importance of optimizing KTP loading to balance specificity and functional performance.

The kidney-targeting peptide exhibits preferential binding to renal proximal tubule cells over other organs, including the liver, though secondary endothelial interactions occur.[43] In our in vitro system, KTP-LNPs demonstrate 3.2-fold selectivity for HRPTEpCs vs fibroblasts and 2.1-fold vs HUVECs, consistent with this physiologic profile (Supplementary Figures S7 and S8). We selected 5-hour uptake timepoints based on standard practice in nanoparticle internalization studies, which often use these early timeframes to assess binding kinetics and determine optimal cellular uptake periods.[42] We suspect this interaction may involve megalin, a well-known endocytic receptor expressed on kidney proximal tubular epithelial cells. This hypothesis is supported by previous reports showing that other kidney-targeting peptides, such as (KKEEE)3 K, bind specifically to megalin and facilitate uptake into epithelial kidney cells.[43] Therefore, it is plausible that KTP recognizes a similar or related receptor, possibly megalin, to achieve its selective targeting. However, further experimental characterization is needed to confirm megalin's involvement in the uptake mechanism and to elucidate the precise nature of the receptor-mediated interaction. Nevertheless, this kidney-biased preference, despite modest liver accumulation and endothelial off-targeting,[43] positions KTP as an optimal ligand for engineering ECFC-kidney selectivity, where backpack-mediated surface presentation converts organ preference into enhanced cell-cell interactions for localized paracrine delivery.

5. CONCLUSIONS

This surface-engineering strategy creates KTP-displaying liposome backpacks on ECFCs, leveraging extracellular attachment while preserving viability, phenotype, and angiogenic function. KTP's renal proximal tubule affinity, despite noted endothelial interactions, positions this platform to potentially enhance kidney-selective paracrine delivery in ischemia models. A targeting strategy is essential to advance ECFCs toward clinical applications, and this modular backpack approach could adapt to other organs, provided the biomaterial is rationally designed not for drug delivery, but to guide cells via surface conjugation.

https://doi.org/10.1021/acsabm.5c02022
ACS Appl. Bio Mater. XXXX, XXX, XXX-XXX

Backpack technology, an emerging frontier in biomaterials, enables modular surface guidance. This targeting strategy moves forward the clinical translation of the ECFCs inspired by biomaterial adaptations from cancer and immunoengineering fields to tissue engineering and regenerative medicine.

■ ASSOCIATED CONTENT

Data Availability Statement

Additional data, which contributed to this study, are present in the Supplementary Data.

Supporting Information

The Supporting Information is available free of charge at https://pubs.acs.org/doi/10.1021/acsabm.5c02022.

The Jupyter Notebook (.ipynb) code used in the study for live/dead assay analysis (PDF)

The calculator used to determine the addition of the −SH group to KTP and the conjugation of KTP to MAE groups on the LNPs (XLSX)

Additional data (DOCX)

GitHub link (DOCX)

■ AUTHOR INFORMATION

Corresponding Author

Donny Hanjaya-Putra − *Department of Aerospace and Mechanical Engineering, Bioengineering Graduate Program, University of Notre Dame, Notre Dame, Indiana 46556, United States; Harper Cancer Research Institute, University of Notre Dame, Notre Dame, Indiana 46617, United States; Department of Chemical and Biomolecular Engineering, University of Notre Dame, Notre Dame, Indiana 46556, United States; Center for Stem Cells and Regenerative Medicine, University of Notre Dame, Notre Dame, Indiana 46556, United States;* orcid.org/0000-0002-5403-544X; Email: dputra1@nd.edu; Tel.: 574-631-2291

Authors

Brenda Cruz-Gonzalez − *Department of Aerospace and Mechanical Engineering, Bioengineering Graduate Program, University of Notre Dame, Notre Dame, Indiana 46556, United States;* orcid.org/0009-0003-0920-9513

Fei Fan − *Department of Aerospace and Mechanical Engineering, Bioengineering Graduate Program, University of Notre Dame, Notre Dame, Indiana 46556, United States;* orcid.org/0000-0002-1738-9150

Eva Hall − *Department of Aerospace and Mechanical Engineering, Bioengineering Graduate Program, University of Notre Dame, Notre Dame, Indiana 46556, United States*

Sanjoy Saha − *Department of Aerospace and Mechanical Engineering, Bioengineering Graduate Program, University of Notre Dame, Notre Dame, Indiana 46556, United States;* orcid.org/0000-0001-6902-683X

Laura S. Haneline − *Herman B. Wells Center for Pediatric Research, Indiana University School of Medicine, Riley Hospital for Children at Indiana University Health, Indianapolis, Indiana 46202, United States*

David P. Basile − *Department of Cellular & Integrative Physiology, Indiana University School of Medicine, Indianapolis, Indiana 46202, United States*

Complete contact information is available at: https://pubs.acs.org/doi/10.1021/acsabm.5c02022

Author Contributions

B.C.-G. and D.H.-P. conceived the study, designed the experiments, interpreted the data, and wrote the manuscript. B.C.-G. and F.F. performed the synthesis and characterization of the nanoparticle experiments and analyzed the data. E.H. and S.S. contributed to the cell culture experimental work and data interpretation. L.S.H. contributed to the conceptual development of the study and provided expertise related to endothelial colony-forming cells. D.P.B. contributed expert knowledge on kidney anatomy, kidney-targeting strategies, and the therapeutic application of ECFCs. All authors reviewed and approved the final manuscript.

Notes

This study did not involve any experiments conducted on either animals or humans.

The authors declare no competing financial interest.

■ ACKNOWLEDGMENTS

We acknowledge support from the University of Notre Dame through the "Advancing Our Vision" Initiative in Stem Cell Research, Harper Cancer Research Institute—American Cancer Society Institutional Research Grant (IRG-17-182-04), American Heart Association through Career Development Award (19-CDA-34630012 to D.H.-P.), National Science Foundation (2047903 to D.H-P.), National Institutes of Health (1R35-GM-143055 to D.H.-P.), and the Center for Environmental Science and Technology Fellowship (CEST Fellowship to B.C.-G). TEM presented in this paper was obtained using the instruments of the Notre Dame Integrated Imaging Facility/NDIIF, University of Notre Dame. FTIR analysis in this paper was conducted using the instrument at the Center for Environmental Science and Technology/CEST, University of Notre Dame. NTA analysis in this paper was conducted by the instrument of Harper Cancer Research Institute/HCRI, University of Notre Dame. We appreciate the support from these facilities for this study.

■ REFERENCES

(1) Liu, Y.; Lyons, C. J.; Ayu, C.; O'Brien, T. Recent advances in endothelial colony-forming cells: from the transcriptomic perspective. *J. Transl. Med.* **2024**, *22* (1), 313.

(2) Collett, J. A.; Mehrotra, P.; Crone, A.; Shelley, W. C.; Yoder, M. C.; Basile, D. P. Endothelial Colony-Forming Cells Ameliorate Endothelial Dysfunction via Secreted Factors Following Ischemia-Reperfusion Injury. *Am. J. Physiol.-Renal Physiol.* **2017**, *312* (5), F897–F907.

(3) Ding, J.; Zhao, Z.; Wang, C.; Wang, C.-X.; Li, P.-C.; Qian, C.; Teng, G.-J. Bioluminescence Imaging of Transplanted Human Endothelial Colony-Forming Cells in an Ischemic Mouse Model. *Brain Res.* **2016**, *1642*, 209–218.

(4) Garrigue, P.; Hache, G.; Bennis, Y.; Brige, P.; Stalin, J.; Pellegrini, L.; Velly, L.; Orlandi, F.; Castaldi, E.; Dignat-George, F.; Sabatier, F.; Guillet, B. Erythropoietin Pretreatment of Transplanted Endothelial Colony-Forming Cells Enhances Recovery in a Cerebral Ischemia Model by Increasing Their Homing Ability: A SPECT/CT Study. *J. Nucl. Med.* **2016**, *57* (11), 1798–1804.

(5) Zhang, Y.; Li, Y.; Wang, S.; Han, Z.; Huang, X.; Li, S.; Chen, F.; Niu, R.; Dong, J.; Jiang, R.; Zhang, J. Transplantation of Expanded Endothelial Colony-Forming Cells Improved Outcomes of Traumatic Brain Injury in a Mouse Model. *J. Surg. Res.* **2013**, *185* (1), 441–449.

(6) Huang, X.-T.; Zhang, Y.-Q.; Li, S.-J.; Li, S.-H.; Tang, Q.; Wang, Z.-T.; Dong, J.-F.; Zhang, J.-N. Intracerebroventricular Transplantation of Ex Vivo Expanded Endothelial Colony-Forming Cells Restores Blood-Brain Barrier Integrity and Promotes Angiogenesis of Mice with Traumatic Brain Injury. *J. Neurotrauma* **2013**, *30* (24), 2080–2088.
(7) Faris, P.; Negri, S.; Perna, A.; Rosti, V.; Guerra, G.; Moccia, F. Therapeutic Potential of Endothelial Colony-Forming Cells in Ischemic Disease: Strategies to Improve Their Regenerative Efficacy. *Int. J. Mol. Sci.* **2020**, *21* (19), No. 7406.
(8) Tripathi, H.; Domingues, A.; Donahue, R.; Cras, A.; Guerin, C. L.; Gao, E.; Levitan, B.; Ratajczak, M. Z.; Smadja, D. M.; Abdel-Latif, A.; Tarhuni, W. M. Combined Transplantation of Human MSCs and ECFCs Improves Cardiac Function and Decrease Cardiomyocyte Apoptosis After Acute Myocardial Infarction. *Stem Cell Rev. Rep.* **2023**, *19* (2), 573–577.
(9) Iqbal, F.; Johnston, A.; Wyse, B.; Rabani, R.; Mander, P.; Hoseini, B.; Wu, J.; Li, R. K.; Gauthier-Fisher, A.; Szaraz, P.; Librach, C. Combination human umbilical cord perivascular and endothelial colony forming cell therapy for ischemic cardiac injury. *NPJ Regen. Med.* **2023**, *8* (1), 45.
(10) Kim, S.-W.; Jin, H. L.; Kang, S.-M.; Kim, S.; Yoo, K.-J.; Jang, Y.; Kim, H. O.; Yoon, Y. Therapeutic Effects of Late Outgrowth Endothelial Progenitor Cells or Mesenchymal Stem Cells Derived from Human Umbilical Cord Blood on Infarct Repair. *Int. J. Cardiol.* **2016**, *203*, 498–507.
(11) Burger, D.; Viñas, J. L.; Akbari, S.; Dehak, H.; Knoll, W.; Gutsol, A.; Carter, A.; Touyz, R. M.; Allan, D. S.; Burns, K. D. Human Endothelial Colony-Forming Cells Protect against Acute Kidney Injury: Role of Exosomes. *Am. J. Pathol.* **2015**, *185* (8), 2309–2323.
(12) Alphonse, R. S.; Vadivel, A.; Fung, M.; Shelley, W. C.; Critser, P. J.; Ionescu, L.; O'Reilly, M.; Ohls, R. K.; McConaghy, S.; Eaton, F.; Zhong, S.; Yoder, M.; Thébaud, B. Existence, Functional Impairment, and Lung Repair Potential of Endothelial Colony-Forming Cells in Oxygen-Induced Arrested Alveolar Growth. *Circulation* **2014**, *129* (21), 2144–2157.
(13) Kang, K.-T.; Lin, R.-Z.; Kuppermann, D.; Melero-Martin, J. M.; Bischoff, J. Endothelial Colony Forming Cells and Mesenchymal Progenitor Cells Form Blood Vessels and Increase Blood Flow in Ischemic Muscle. *Sci. Rep.* **2017**, *7*, 770.
(14) Lin, R.-Z.; Moreno-Luna, R.; Li, D.; Jaminet, S.-C.; Greene, A. K.; Melero-Martin, J. M. Human Endothelial Colony-Forming Cells Serve as Trophic Mediators for Mesenchymal Stem Cell Engraftment via Paracrine Signaling. *Proc. Natl. Acad. Sci. U. S. A.* **2014**, *111* (28), 10137–10142.
(15) Melero-Martin, J. M. Human Endothelial Colony-Forming Cells. *Cold Spring Harb. Perspect. Med.* **2022**, *12* (12), No. a041154.
(16) Rojas-Torres, M.; Sánchez-Gomar, I.; Rosal-Vela, A.; Beltrán-Camacho, L.; Eslava-Alcón, S.; Alonso-Piñeiro, J. Á.; Martín-Ramírez, J.; Moreno-Luna, R.; Durán-Ruiz, M. C. Assessment of Endothelial Colony Forming Cells Delivery Routes in a Murine Model of Critical Limb Threatening Ischemia Using an Optimized Cell Tracking Approach. *Stem Cell Res. Ther.* **2022**, *13*, 266.
(17) Cruz-Gonzalez, B.; Johandes, E.; Gramm, D.; Hanjaya-Putra, D. Bottom-up Biomaterial Strategies for Creating Tailored Stem Cells in Regenerative Medicine. *Front. Bioeng. Biotechnol.* **2025**, *13*, No. 1581292.
(18) Wyatt Shields, C.; Evans, M. A.; Wang, L. L.-W.; et al. Cellular backpacks for macrophage immunotherapy. *Sci. Adv.* **2020**, *6*, No. eaaz6579.
(19) Bui, L.; Edwards, S.; Hall, E.; Alderfer, L.; Round, K.; Owen, M.; Sainaghi, P.; Zhang, S.; Nallathamby, P. D.; Haneline, L. S.; Hanjaya-Putra, D. Engineering Bioactive Nanoparticles to Rejuvenate Vascular Progenitor Cells. *Commun. Biol.* **2022**, *5* (1), 635.
(20) Mahdi, F.; Chade, A. R.; Bidwell, G. L. Utilizing a Kidney-Targeting Peptide to Improve Renal Deposition of a Pro-Angiogenic Protein Biopolymer. *Pharmaceutics* **2019**, *11* (10), 542.
(21) Bidwell, G. L.; Mahdi, F.; Shao, Q.; Logue, O. C.; Waller, J. P.; Reese, C.; Chade, A. R. A Kidney-Selective Biopolymer for Targeted Drug Delivery. *Am. J. Physiol. Renal Physiol.* **2017**, *312* (1), F54–F64.
(22) Chade, A. R.; Bidwell, G. L. Novel Drug Delivery Technologies and Targets for Renal Disease. *Hypertension* **2022**, *79* (9), 1937–1948.
(23) Zhang, Q.; Duncan, S.; Szulc, D. A.; Kutryk, M. J. B. Antibody Functionalized Intravascular Devices Combined with Genetically Engineered Endothelial Colony-Forming Cells for Targeted Drug Delivery: A Proof-of-Concept Study. *Eur. J. Pharm. Biopharm.* **2022**, *181*, 218–226.
(24) S. Bashth, O.; A. Elkhodiry, M.; Laroche, G.; A. Hoesli, C. Surface Grafting of Fc-Binding Peptides as a Simple Platform to Immobilize and Identify Antibodies That Selectively Capture Circulating Endothelial Progenitor Cells. *Biomater. Sci.* **2020**, *8*, 5465–5475.
(25) Hao, D.; Xiao, W.; Liu, R.; Kumar, P.; Li, Y.; Zhou, P.; Guo, F.; Farmer, D. L.; Lam, K. S.; Wang, F.; Wang, A. Discovery and Characterization of a Potent and Specific Peptide Ligand Targeting Endothelial Progenitor Cells and Endothelial Cells for Tissue Regeneration. *ACS Chem. Biol.* **2017**, *12* (4), 1075–1086.
(26) Tian, Y.; Seeto, W. J.; Páez-Arias, M. A.; Hahn, M. S.; Lipke, E. A. Endothelial Colony Forming Cell Rolling and Adhesion Supported by Peptide-Grafted Hydrogels. *Acta Biomater.* **2022**, *152*, 74–85.
(27) Basile, D. P.; Yoder, M. C. Renal Endothelial Dysfunction in Acute Kidney Ischemia Reperfusion Injury. *Cardiovasc. Hematol. Disord. Drug Targets* **2014**, *14* (1), 3–14.
(28) Ingram, D. A.; Lien, I. Z.; Mead, L. E.; Estes, M.; Prater, D. N.; Derr-Yellin, E.; DiMeglio, L. A.; Haneline, L. S. In vitro hyperglycemia or a diabetic intrauterine environment reduces neonatal endothelial colony-forming cell numbers and function. *Diabetes* **2008**, *57* (3), 724–731.
(29) Paschalaki, K.; Pericleous, C. Isolation and Characterization of Endothelial-Colony Forming Cells (ECFC): Studying Endothelial Senescence for Translational Studies and for Personalized Medicine. *Methods Mol. Biol.* **2025**, *2906*, 255–270.
(30) Stephan, M. T.; Moon, J. J.; Um, S. H.; Bershteyn, A.; Irvine, D. J. Therapeutic Cell Engineering with Surface-Conjugated Synthetic Nanoparticles. *Nat. Med.* **2010**, *16* (9), 1035–1041.
(31) Utterström, J.; Barriga, H. M. G.; Holme, M. N.; Selegård, R.; Stevens, M. M.; Aili, D. Peptide-Folding Triggered Phase Separation and Lipid Membrane Destabilization in Cholesterol-Rich Lipid Vesicles. *Bioconjug. Chem.* **2022**, *33* (4), 736–746.
(32) Lim, S. K.; Sandén, C.; Selegård, R.; Liedberg, B.; Aili, D. Tuning Liposome Membrane Permeability by Competitive Peptide Dimerization and Partitioning-Folding Interactions Regulated by Proteolytic Activity. *Sci. Rep.* **2016**, *6*, No. 21123.
(33) Smith, W. J.; Tran, H.; Griffin, J. I.; Jones, J.; Vu, V. P.; Nilewski, L.; Gianneschi, N.; Simberg, D. Lipophilic Indocarbocyanine Conjugates for Efficient Incorporation of Enzymes, Antibodies and Small Molecules into Biological Membranes. *Biomaterials* **2018**, *161*, 57–68.
(34) Tyler, A.; Greenfield, J. L.; Seddon, J. M.; Brooks, N. J.; Purushothaman, S. Coupling Phase Behavior of Fatty Acid Containing Membranes to Membrane Bio-Mechanics. *Front. Cell Dev. Biol.* **2019**, *7*, 187.
(35) Ohta, T.; Yamada, R.; Fujita, S.; Takahata, T.; Shiba, K.; Machida, S.; Tate, S. DOPG Small Unilamellar Vesicles Function as Nano-Carriers Targeting the Clustered Lectin-like Oxidized LDL Receptor (LOX-1) on the Cell Surface. *J. Drug Deliv. Sci. Technol.* **2019**, *51*, 327–336.
(36) Rawal, M.; Singh, A.; Amiji, M. M. Quality-by-Design Concepts to Improve Nanotechnology-Based Drug Development. *Pharm. Res.* **2019**, *36* (11), 153.
(37) Soo, C. Y.; Song, Y.; Zheng, Y.; Campbell, E. C.; Riches, A. C.; Gunn-Moore, F.; Powis, S. J. Nanoparticle Tracking Analysis Monitors Microvesicle and Exosome Secretion from Immune Cells. *Immunology* **2012**, *136* (2), 192–197.

https://doi.org/10.1021/acsabm.5c02022
ACS Appl. Bio Mater. XXXX, XXX, XXX-XXX

(38) Wiśniewski, J R; Gaugaz, F. Z. Fast and Sensitive Total Protein and Peptide Assays for Proteomic Analysis. *Anal. Chem.* **2015**, *87* (8), 4110–4116.
(39) Sinha, S.; Sachar, H. S.; Das, S. Electrostatically Motivated Design of Biomimetic Nanoparticles: Promoting Specific Adhesion and Preventing Nonspecific Adhesion Simultaneously. *Appl. Phys. Lett.* **2018**, *112*, 243702.
(40) Kuodis, Z.; Matulaitienė, I.; Špandyreva, M.; Labanauskas, L.; Stončius, S.; Eicher-Lorka, O.; Sadzevičienė, R.; Niaura, G. Reflection Absorption Infrared Spectroscopy Characterization of SAM Formation from 8-Mercapto-N-(phenethyl)octanamide Thiols with Phe Ring and Amide Groups. *Molecules* **2020**, *25*, 5633.
(41) Cobb, J. S.; Zai-Rose, V.; Correia, J. J.; Janorkar, A. V. FT-IR Spectroscopic Analysis of the Secondary Structures Present during the Desiccation Induced Aggregation of Elastin-Like Polypeptide on Silica. *ACS Omega* **2020**, *5* (14), 8403–8413.
(42) Zhang, Q.; Cannavicci, A.; Kutryk, M. J. B. Exploring Endothelial Colony-Forming Cells to Better Understand the Pathophysiology of Disease: An Updated Review. *Stem Cells Int.* **2022**, *2022* (1), No. 4460041.
(43) Pasqualini, R.; Ruoslahti, E. Organ Targeting In Vivo Using Phage Display Peptide Libraries. *Nature* **1996**, *380* (6572), 364–366.
(44) Wang, G.; Li, Q.; Chen, D.; Wu, B.; Wu, Y.; Tong, W.; Huang, P. Kidney-Targeted Rhein-Loaded Liponanoparticles for Diabetic Nephropathy Therapy via Size Control and Enhancement of Renal Cellular Uptake. *Theranostics* **2019**, *9* (21), 6191–6208.
(45) Gu, X.-R.; Liu, K.; Deng, Y.-X.; Xiang, B.-X.; Zhou, L.-Y.; Yin, W.-J.; Huang, J.-X.; Meng, Y.-C.; Li, D.-K.; Que, R.-M.; Tang, Z.-Y.; Zhou, G.-L.; Wu, Y.-F.; Huang, Y.-J.; Zhou, W.-H.; Zuo, X.-C. A Renal-Targeted Gene Delivery System Derived from Spermidine for Arginase-2 Silencing and Synergistic Attenuation of Drug-Induced Acute Kidney Injury. *Chem. Eng. J.* **2024**, *486*, No. 150125.
(46) Martínez-Jothar, L.; Doulkeridou, S.; Schiffelers, R. M.; Sastre Torano, J.; Oliveira, S.; van Nostrum, C. F.; Hennink, W. E. Insights into maleimide-thiol conjugation chemistry: Conditions for efficient surface functionalization of nanoparticles for receptor targeting. *J. Control. Release* **2018**, (28),*282*, 101–109.
(47) Jones, D. S.; Rowe, C. G.; Chen, B.; Reiter, K.; Rausch, K. M.; Narum, D. L.; Wu, Y.; Duffy, P. E. A Method for Producing Protein Nanoparticles with Applications in Vaccines. *PLoS One* **2016**, *11* (3), No. e0138761.
(48) Liu, Y.; Fang, J.; Kim, Y. J.; Wong, M. K.; Wang, P. Codelivery of doxorubicin and paclitaxel by cross-linked multilamellar liposome enables synergistic antitumor activity. *Mol. Pharm.* **2014**, *11* (5), 1651–1661.
(49) Kraft, J. C.; Freeling, J. P.; Wang, Z. iyao; Ho, R. J. Y. Emerging Research and Clinical Development Trends of Liposome and Lipid Nanoparticle Drug Delivery Systems. *J. Pharm. Sci.* **2014**, *103* (1), 29–52.
(50) Arakelian, L.; Lion, J.; Churlaud, G.; Bargui, R.; Thierry, B.; Mutabazi, E.; Bruneval, P.; Alberdi, A. J.; Doliger, C.; Veyssiere, M.; Larghero, J.; Mooney, N. Endothelial CD34 Expression and Regulation of Immune Cell Response In-Vitro. *Sci. Rep.* **2023**, *13* (1), 13512.

https://doi.org/10.1021/acsabm.5c02022
ACS Appl. Bio Mater. XXXX, XXX, XXX-XXX